UTX Regulates Human Neural Differentiation and Dendritic Morphology by Resolving Bivalent Promoters

Qing-Yuan Tang,[1,2,3] Shuang-Feng Zhang,[1,2,3] Shang-Kun Dai,[1,2,3] Cong Liu,[1,2,3] Ying-Ying Wang,[1,2,3] Hong-Zhen Du,[1,3] Zhao-Qian Teng,[1,2,3,*] and Chang-Mei Liu[1,2,3,*]

[1]State Key Laboratory of Stem Cell and Reproductive Biology, Institute of Zoology, Chinese Academy of Sciences, Beijing 100101, China
[2]Savaid Medical School, University of Chinese Academy of Sciences, Beijing 100049, China
[3]Institute for Stem Cell and Regeneration, Chinese Academy of Sciences, Beijing 100101, China
*Correspondence: tengzq@ioz.ac.cn (Z.-Q.T.), liuchm@ioz.ac.cn (C.-M.L.)
https://doi.org/10.1016/j.stemcr.2020.06.015

SUMMARY

UTX, a H3K27me3 demethylase, plays an important role in mouse brain development. However, so little is known about the function of *UTX* in human neural differentiation and dendritic morphology. In this study, we generated *UTX*-null human embryonic stem cells using CRISPR/Cas9, and differentiated them into neural progenitor cells and neurons to investigate the effects of *UTX* loss of function on human neural development. The results showed that the number of differentiated neurons significantly reduced after loss of *UTX*, and that the dendritic morphology of *UTX* KO neurons tended to be simplified. The electrophysiological recordings showed that most of the *UTX* KO neurons were immature. Finally, RNA sequencing identified dozens of differentially expressed genes involved in neural differentiation and synaptic function in *UTX* KO neurons and our results demonstrated that *UTX* regulated these critical genes by resolving bivalent promoters. In summary, we establish a reference for the important role of *UTX* in human neural differentiation and dendritic morphology.

INTRODUCTION

Epigenetic regulations, which include DNA methylation, genomic imprinting, RNA editing, and histone modification, have been reported playing critical roles in almost every biological process (Bird, 2002; Jenuwein and Allis, 2001; Tsankova et al., 2007). Trimethylation of histone H3 at lysine 27 (H3K27me3) is believed to be a repressive epigenetic mark for maintaining transcriptional gene silencing (Stewart-Morgan et al., 2020). In mammals, the dynamic steady-state levels of di-methylation and tri-methylation of histone H3 lysine 27 (H3K27me2/3) are mainly regulated by the balance between the methyltransferase polycomb repressor complex 2 (PRC2) and the histone demethylases *UTX* (also known as *KDM6A*) and *JMJD3* (also known as *KDM6B*) (Agger et al., 2007; Lan et al., 2007; Margueron and Reinberg, 2011; Swigut and Wysocka, 2007). Trimethylated histone H3 lysine 27 (H3K27me3) is critical for wound repair, skeleton growth, and cell fate determination (Ezhkova et al., 2011; Wei et al., 2009; Zhang et al., 2015). Meanwhile, the JMJC domain protein *UTX* acts as an H3K27-specific demethylases that remove this H3K37me mark, enabling the activation of genes involved in cancer, germ cell epigenetic reprogramming, and inflammation (Grasso et al., 2012; Kruidenier et al., 2012; Mansour et al., 2012).

H3K27me3 is a mark of gene repression, while H3K4me3 is a mark of gene activation. These two marks denoting opposite gene expression states co-localize at many differentiation-specific gene promoters in stem cells to form bivalent promoters in which they are located at different H3 tails in nucleosomes (Blanco et al., 2020; Minoux et al., 2017). The H3K4 methyltransferase mixed-lineage leukemia 2 (*MLL2*; also known as *KMT2B*) is important for the formation of H3K4me3 in bivalent domains, and the H3K4 methyltransferase *MLL1* plays a redundant role in depositing H3K4me3 to generate bivalent domains (Denissov et al., 2014; Hu et al., 2013). Besides, the H3K27 methyltransferase complex PRC2 and H3K4 methyltransferases *SET1A* and *SET1B* are associated with the generation of bivalency (Voigt et al., 2013). However, we still know very little about which histone methylation modifier is responsible for the resolution of bivalent domains into active monovalent states during human neural differentiation.

Previous studies have demonstrated that the regulation of H3K27me3 is absolutely indispensable for the development and function of the mammalian nervous system (Aldiri et al., 2017; Ayata et al., 2018; Henriquez et al., 2013; Liu et al., 2017). For example, *Ezh2*, a histone methyltransferase of PRC2, is essential for controlling the rate at which cortical progenitor cells proliferate and differentiate into lineage cells, and loss of *Ezh2* results in a removal of the repressive mark of H3K27me3 in cortical progenitor cells and a decline in terminally differentiated neurons (Pereira et al., 2010). During neocortical development, the polycomb group complex restricts neurogenic competence of neural progenitor cells (NPCs) and promotes the fate transition of NPCs from neurogenic to astrogenic (Hirabayashi et al., 2009). *UTX* is broadly expressed in various regions of the mouse brain (Xu et al., 2008), and its mutations are associated with Kabuki syndrome whose patients have
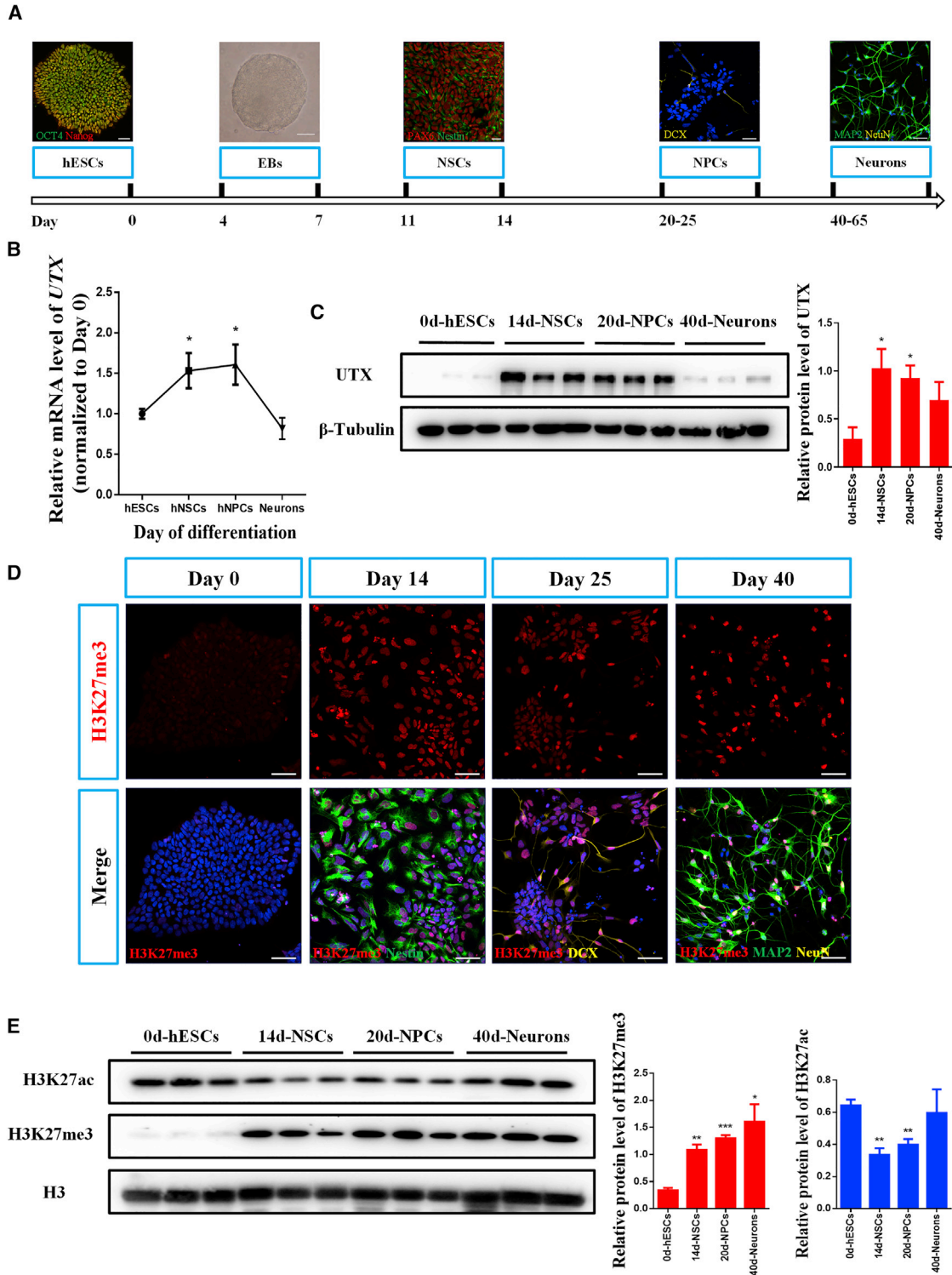
Figure 1. *UTX* **Is Upregulated in Earlier Stages of Neural Differentiation of hESCs**

(A) Schematic illustration of neural differentiation of hESCs. hESCs, human embryonic stem cells; EB, embryoid bodies; hNSCs, human neural stem cells; hNPCs, human neural progenitor cells. Scale bar, 50 μm.

(B) Real-time PCR analysis showing higher mRNA levels of *UTX* in earlier stages of neural differentiation of hESCs. *GAPDH* is used as an internal control for real-time PCR.

(legend continued on next page)

developmental delay and intellectual disability (Miyake et al., 2013). In addition, *UTX* has also been demonstrated to be the promotional transcription factor of *Pten* by demethylating H3K27me3 at the *Pten* promoter to control neurogenesis in mice (Lei and Jiao, 2018). However, some other findings suggest that the H3K27me demethylase activity of *UTX* is dispensable for the development of the nervous system. For instance, Kabuki causative point mutations upstream of the JmjC domain do not destroy *UTX* demethylation (Shpargel et al., 2017). In addition, deletion of *UTX* does not affect global H3K27me levels in neural crest cells (Shpargel et al., 2017). Therefore, whether the regulation mechanism of *UTX* in neurodevelopment depends on its demethylase function remains to be investigated.

In our previous study, we found that specific deletion of *UTX* in the mouse forebrain results in aberrant dendrite complexity and abnormal synaptic plasticity, and H3K27me3 level increased in the hippocampus of *UTX* knockout (KO) mice (Tang et al., 2017). However, the role and mechanism of *UTX* in human neural morphogenesis and development have not yet been elucidated. In this study, we investigated the role of *UTX* in neural progenitors and neurons differentiated from human embryonic stem cells (hESCs). We found that *UTX* was upregulated upon neural differentiation of hESCs, and loss of *UTX* in hESCs led to the decline in their differentiation potential into neurons, the decrease of neurite complexity, and the defect of electrophysiological function. Finally, we provided evidence showing that *UTX* regulated human neural differentiation and dendritic morphology of neurons by resolving bivalent promoter dependent on its H3K27 demethylase activity.

RESULTS

UTX Is Enriched in Human NPCs during Differentiation of hESCs into Neurons

To investigate the expression of *UTX* and H3K27me3 during human neural differentiation, we utilized an *in vitro* culture system to differentiate hESCs into human neural stem cells (hNSCs), human neural progenitor cells (hNPCs), and neurons (Figure 1A). Real-time RT-PCR analysis showed that the mRNA expression of *UTX* was not abundant in hESCs, but was increased in hNSCs and hNPCs (Figure 1B). Consistent with this, higher protein

levels of *UTX* in hNSCs and hNPCs were also detected by western blotting (Figure 1C). Although *UTX* is known to have histone demethylase activity, both immunofluorescence and western blotting assays demonstrated that the expression levels of both H3K27me3 and *UTX* were also significantly increased during the neural differentiation of hESCs (Figures 1D and 1E). Meanwhile, the expression of H3K27ac was declined by almost 30% in hNSCs and hNPCs (Figure 1E). These results suggested that *UTX* might play an important role in neural differentiation of hESCs.

The Expression of H3K27me3 Is Not Altered in *UTX* KO hESCs

To explore the function of UTX in neural differentiation of hESCs, we conducted CRISPR/Cas9-mediated gene editing to knock out *UTX* in hESCs. We successfully established two *UTX*-null hESC clones (KO1, KO2) (Figure 2A). Two specific single-guide RNA (sgRNAs) targeting exon 1 of *UTX* were designed (as shown in Figure 2A and at the Optimized CRISPR Design website http://crispr.mit.edu) (Cong et al., 2013). Off-target effect was not detected in six potential genes that were predicted by the Optimized CRISPR Design tool, indicating the specificity of the selected sgRNAs (Figure S1A).

To confirm the deletion of *UTX* in hESCs, we performed western blotting, RT-PCR, and immunofluorescent staining analyses of *UTX* KO clones. Compared with wild-type (WT) cells, we observed a complete loss of UTX protein both in KO1 and KO2 hESCs (Figures 2B and 2D). Consistent with this, the mRNA expression of *UTX* was almost undetectable in *UTX* KO hESCs (Figure 2C). Next, we examined the expression of H3K27me3 in *UTX* KO hESCs, and found that H3K27me3 was unchanged upon the deletion of *UTX* in hESCs (Figures 2E and 2F). Besides, the expression of *JMJD3*, another H3K27me3 demethylase, was not changed in *UTX* KO hESCs (Figure S1B) and two *UTX* knockout cell lines had a normal karyotype (Figure S1C). In summary, these observations supported the idea that UTX might play roles independent of its histone lysine demethylase activity in hESCs.

Deletion of *UTX* Has No Effects on Pluripotency and Self-Renewal of hESCs

To confirm the pluripotency status of the established *UTX* KO hESC clones, we examined the expression of several

---

(C) Western blotting indicating upregulated protein levels of *UTX* at earlier stages during neural differentiation of hESCs. β-Tubulin is used as a loading control.

(D) Representative images of H3K27me3 immunostaining at different stages of neural differentiation of hESCs. DAPI, a nuclei marker; *Nestin*, an NSC marker; *DCX*, an NPCs marker; *MAP2*, a mature neuron marker. Scale bar, 50 μm.

(E) Western blotting showing protein levels of H3K27me3 and H3K27ac upon neural differentiation of hESCs. Histone 3 was used as a loading control.

Results are presented as mean ± SEM; n ≥ 3 independent experiments. *p < 0.05, **p < 0.01, ***p < 0.001.

(legend on next page)

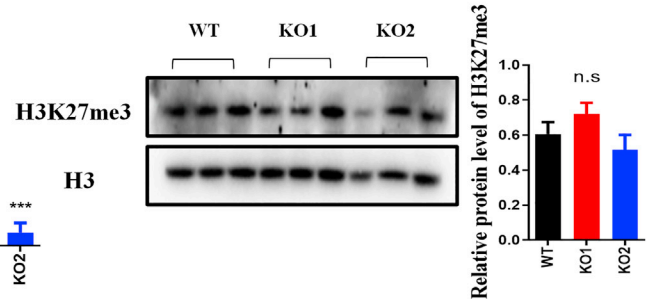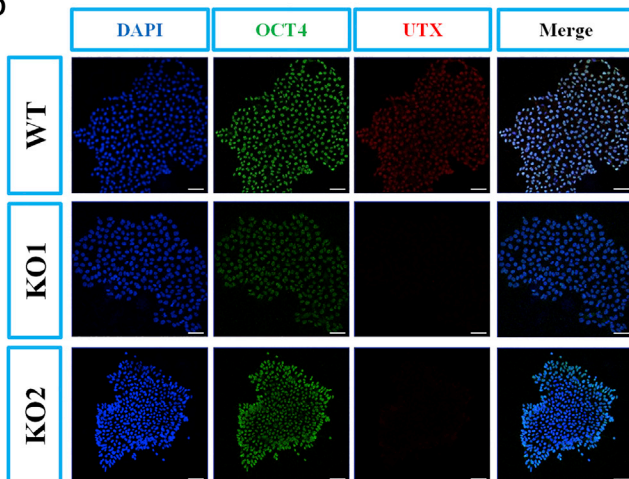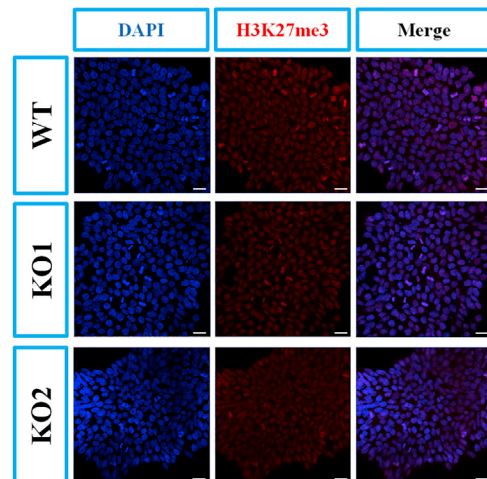markers for stemness and cell proliferation. We observed similar expression levels of pluripotency markers in *UTX* WT and KO cell lines by immunofluorescence staining, qPCR, and western blotting (Figures S2A–S2C). *UTX* WT and KO cells also displayed similar proliferation potentials by 5-bromo-2′-deoxyuridine (BrdU) incorporation and PH3S10 immunofluorescent staining analyses (Figures S3A and S3B). These results suggested that *UTX* deletion did not affect pluripotency or self-renewal of hESCs.

UTX Is Required for Neural Differentiation of hESCs

We next induced hESCs to differentiate toward hNSCs to investigate the function of *UTX* during early neural differentiation of hESCs. At day 14 after neural differentiation, both *UTX* WT and KO hNSCs could express the typical neural progenitor-specific markers *PAX6* and *Nestin*, with no discernible difference in the percentage of *PAX6*+ or the fluorescence of *Nestin*+ cells (Figures S4A–S4C). RT-PCR results then confirmed that both *UTX* WT and KO hNSCs had the same mRNA expression levels of *PAX6* and *Nestin* (Figure S4E).

Quantification of BrdU+ cells after pulse labeling indicated that *UTX* loss of function had no obvious effect on the proportion of BrdU+ cells compared with WT hNSCs (Figures S4A and S4D). However, at day 40 after neural differentiation, we observed decreased numbers of *MAP2*+ neurons and *Tuj1*+ neurons in both *UTX* KO clones (Figures 3A and 3B), indicating that *UTX* loss of function decreased neural differentiation efficiency of hNSCs. Moreover, our RT-PCR analysis showed a significant decrease in mRNA expression levels of *MAP2* and *TUJ1* in *UTX* KO cells compared with WT control at day 40 after neural differentiation of hESCs (Figure 3C), further proving that deletion of *UTX* inhibited neural differentiation of hESCs.

Loss of UTX Results in Decreased Neurite Complexity and Electrophysiological Defects in hESC-Derived Neurons

We next determined whether the loss of *UTX* affected neurite growth of hESC-derived neurons. Morphology analysis showed that *UTX* KO hESC-derived neurons exhibited a significant reduction in neurite complexity with decrease in total neurite length, and numbers of nodes and ends, compared with WT neurons at day 40 after neural differentiation (Figures 4A–4E).

To further examine the effect of *UTX* loss of function on the maturity of hESC-derived neurons, we performed electrophysiological recordings of hESC-derived neurons in each group using whole-cell patch recordings at day 60 (ASV 0 nM, n = 28; 50 nM, n = 20; 100 nM, n = 26; 1,000 nM) (Figure 4F). We found that, in the WT group, 27.7% of the recorded mature action potential (AP) firing properties with faster and consistent AP velocity, and 36.1% fire single or fewer spikes of APs, 36.1% of the recorded cells fail to show spikes of APs (Figure 4G). As expected, the proportion of immature neurons and no-spike cells increased in both *UTX* KO1 (52.9%) and KO2 (68.7%) cell lines, again suggesting that loss of *UTX* affects the maturity of hESC-derived neurons (Figure 4G). Moreover, membrane resistance (Figure 4I), membrane capacitance (Figure 4J), and sodium/potassium current (Figures 4K–4N) exhibited downward trends in *UTX* KO hESC-derived neurons compared with the control cells, indicating that hESC-derived neurons lacking *UTX* have impaired electrophysiological features.

### Loss of UTX Leads to an Abnormal Transcription Profile in hESC-Derived Neurons

To understand the molecular mechanisms underlying the decreased neurite complexity and electrophysiological defects in *UTX* KO hESC-derived neurons, we performed RNA sequencing (RNA-seq) of hESC-derived neurons at day 40 after neural differentiation. RNA-seq data analysis showed that the transcription profile of *UTX* KO neurons was significantly different from that of control cells (Figure S5A). The clustering analysis and principal-component analysis proved clear discrimination between the *UTX* KO group and the WT group, indicating that neurons displayed distinctly gene expression pattern under the loss of *UTX* (Figures S5B and S5C). A total of 954 downregulated genes and 2,611 upregulated genes were identified in *UTX* KO neurons (Figure S5A). Gene ontology analysis showed that upregulated genes in *UTX* KO neurons were enriched for several cellular biological processes, including

---

**Figure 2. Generation and Characterization of *UTX* Knockout hESCs**

(A) CRISPR sgRNA sequences and mutations in two *UTX* knockout clones (KO1, KO2). The sgRNA sequences are labeled in blue and PAM recognition sequences are highlighted in red. Light-colored sequences indicating the deletion of allele 1 (al1) and allele 2 (al2). WT, wild type.

(B) Western blotting demonstrating that UTX protein is undetectable in both *UTX* KO clones.

(C) Real-time PCR analysis confirming the mutation of *UTX* in both *UTX* KO clones.

(D) Representative images of *UTX* immunostaining of *UTX* KO hESCs. Scale bar, 20 μm.

(E) Western blotting indicating normal protein expression of H3K27me3 in *UTX* KO clones. Histone 3 was used as a loading control.

(F) Representative images of H3K27me3 immunostaining showing its unaltered expression in *UTX* KO clones. Results are presented as mean ± SEM; n = 3 independent experiments. **p < 0.01, ***p < 0.001.
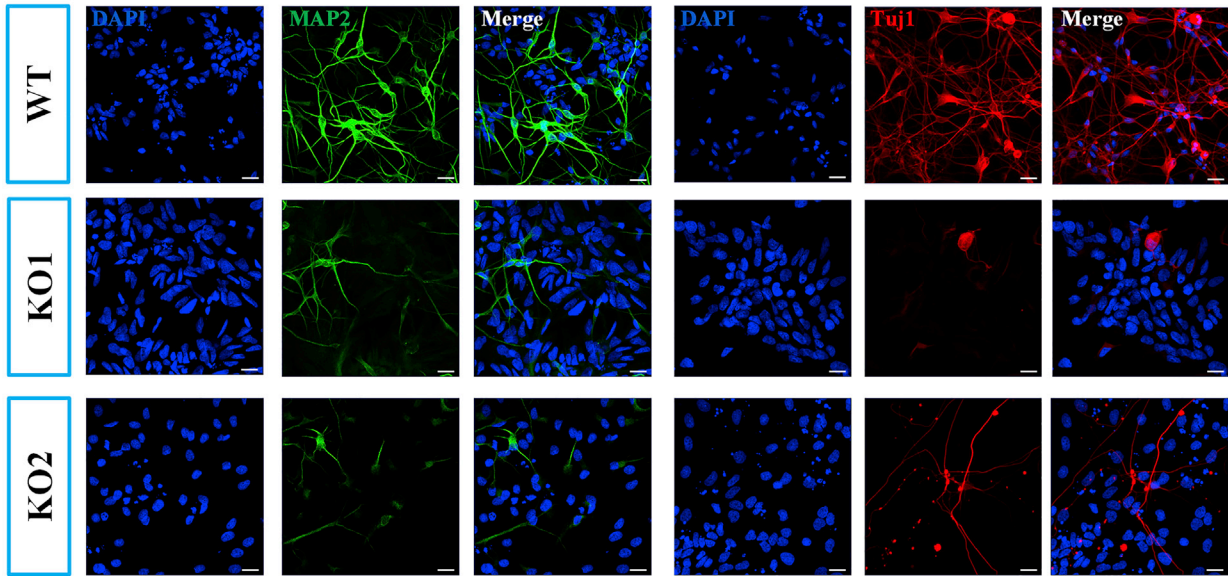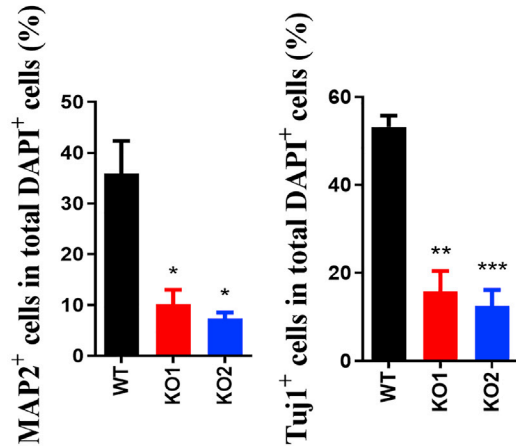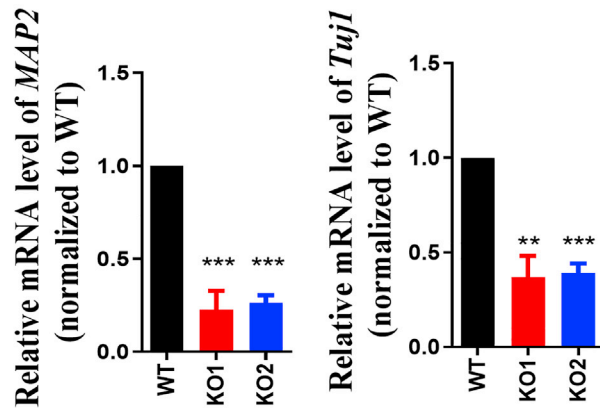
Figure 3. *UTX* Loss-of-function Inhibits Neural Differentiation of hESCs

(A) Immunostaining of neuron markers *MAP2* and *Tuj1* at day 40 of neural differentiation. Scale bar, 20 μm.

(B) Quantitative analysis showing reduced percentages of *MAP2*+ and *Tuj1*+ neurons derived from *UTX* KO hESCs.

(C) qRT-PCR analysis showing that the expression levels *MAP2* and *Tuj1* were significantly lower in *UTX* KO cells at day 40 of neural differentiation. Results are presented as mean ± SEM; n = 3 independent experiments. *p < 0.05, **p < 0.01, ***p < 0.001.

extracellular matrix organization, bone development and mesenchymal cell differentiation, and transforming growth factor β (*TGF-β*) signaling pathway (Figure 5A). Meanwhile, downregulated genes in *UTX* KO neurons were enriched for neurotransmitter transport, signal release from synapse, and neuron fate commitment (Figure 5B). Kyoto Encyclopedia of Genes and Genomes (KEGG) analysis further demonstrated that many downregulated genes in *UTX* KO neurons contributed to glutama-

tergic, dopaminergic, GABAergic, or cholinergic synapse pathway enrichment (Figures S5D and S5E). In contrast, KEGG analysis showed that the upregulated genes in *UTX* KO neurons were enriched in the *TGF-β* signaling pathway (Figures S5D and S5E), a well-known pathway which regulates a diverse range of biological processes during development and adult tissue homeostasis. Finally, we validated the differential expression of 25 genes which were randomly selected from genes positively participated
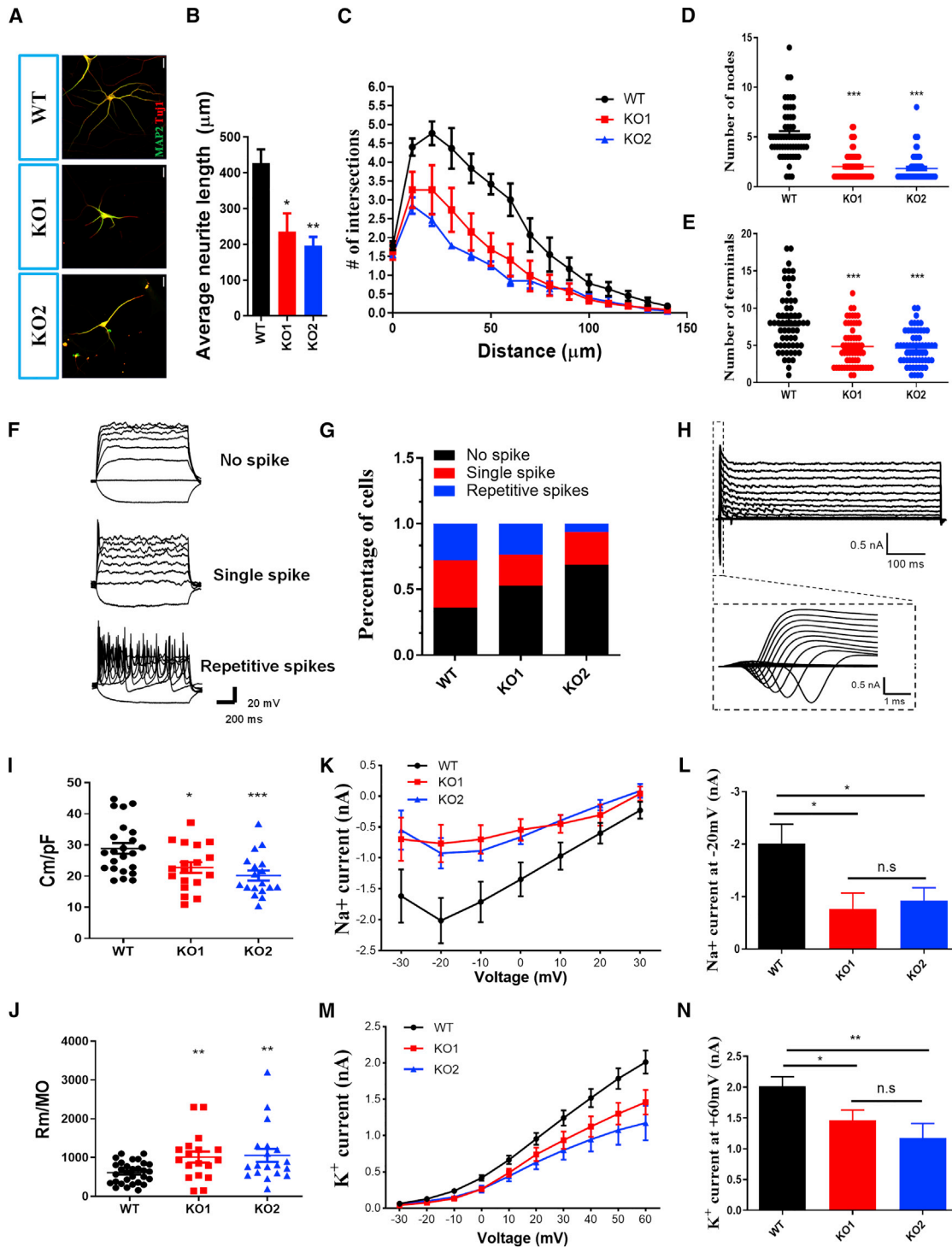
Figure 4. Loss of *UTX* Results in Decreased Neurite Complexity and Electrophysiological Defects of hESC-Derived Neurons

(A) Representative images of neurons derived from *UTX* WT and KO hESCs at day 40 of neural differentiation.

(B) Sholl analysis showing that total neurite length reduced in *UTX* KO hESC-derived neurons (60 neurons in every group in 3 independent experiments).

(C–E) Compared with WT group, *UTX* KO hESC-derived neurons exhibited decreased dendritic complexity as shown in reduced numbers of intersections (C), nodes (D), and ends (E).

(legend continued on next page)

in synaptic function (Figure 5D), neural development (Figure 5E), or *TGF-β* signaling pathway (Figure 5F) using qPCR. These results suggest that *UTX* is a critical regulator for human neural development and synaptic function.

UTX KO Results in H3K27me3 Accumulation and H3K36me3 Reduction in hESC-Derived Neurons

To better understand the regulatory mechanism of *UTX* in hESC-derived neurons, we performed chromatin immunoprecipitation sequencing (ChIP-seq) to analyze the abundance of histone modifications in gene promoters. Meta-analysis of ChIP-seq data showed that both *UTX* KO and WT neurons displayed a broad distribution of H3K27me3 and H3K36me3 in promoters (±5 kb from the transcription start site [TSS]), and there was a slight reduction in H3K27me3, but an obvious reduction in H3K36me3 at the TSS regions (Figures 6A and S6A). We then focused on 1,695 increased peaks of H3K27me3 enrichment (Figure 6B), and found these increased peaks most distributed in gene bodies and promoters (Figure 6C). Furthermore, gene set enrichment analysis showed these H3K27me3-gained regions tended to lose H3K36me3 enrichment (Figures 6D and S6B). Reactome pathway enrichment analysis indicated these gained H3K27me3 peaks were mostly associated with neuronal system, voltage-gated potassium channel, and transmission across chemical synapses, and so on (Figure 6E). To further explore the regulatory mechanism of *UTX*, we performed conjoint data analysis of Chip-seq and RNA-seq, and found that there were 70 downregulated genes from RNA-seq analysis that gained H3K27me3 enrichment after the loss of *UTX* (Figure 6F). Moreover, odds ratio analysis and BETA plot of combined computational analysis showed that the decreased expression of these genes was obviously correlated with the gain of H3K27me3 (Figures 6G and S6C). Gene ontology enrichment analysis of these 70 genes showed that they are involved in forebrain development, hindbrain development, neurotransmitter transport, and signal release from synapse (Figure 6H). *CKB* and *ASIC1* are important for neural development and synaptic function (Inoue et al., 2004; Wemmie et al., 2003), and a reduced H3K36me3 enrichment and an increased H3K27me3 enrichment at promoters of these two genes were detected in *UTX* KO neurons compared with that of WT neurons. Therefore, our results demonstrated that *UTX* regulated transcription of genes associated with neural development and synaptic function depending on its demethylase.

UTX Acts as a Demethylase in Resolution and Activation of Bivalent Promoters during the Neural Differentiation of hESCs

Because H3K27 methyltransferase complex PRC2 was associated with the generation of bivalency (Jadhav et al., 2016), we further assessed the effect of *UTX* loss on bivalent gene expression. Firstly, we used ChromHMM to model the chromatin states in NPCs, which included a bivalent promoter in the fifth row (Figure 7A, left), and analyzed the distribution of all promoters of differentiated genes after the loss of *UTX*. Because *EZH2* and CpG islands have been proven to be enriched in the bivalent promoters (Beguelin et al., 2016; Mantsoki et al., 2015), we used them as positive controls. Interestingly, we found that different expressed genes between *UTX* KO and WT neurons, which could be divided into six groups: (1) RNA-up, (2) K27-down, (3) RNA-up and K27-down, (4) RNA-down, (5) K27-up, and (6) RNA-down and K27-up. Promoters of these six groups all belonged to bivalent promoters compared with control groups (Figure 7A, right). As the combination of transcription factors is also a key step in activating bivalent promoters, we then compared the 70 differentiated genes which belonged to RNA-down and K27-up groups with the *Homo sapiens* TF database, and found that 8 critical TFs were intersected, including *ASCL1*, *POU3F3*, and *POU3F4*, which are important for neural differentiation and morphogenesis (Figure 7B). We then compared the H3K27me3 changes of bivalent promoters of these 70

(F) Representative traces of membrane potential responding to step depolarization by current injection steps from −10 pA to +60 pA in 10-pA increments. Membrane potential was current-clamped at around -65 mV. Representative traces were displayed by WT neurons.

(G) Quantification of the neuron maturity by recorded AP firing patterns at day 60 after differentiation (more than 15 neurons in every group have been recorded).

(H) Representative traces of whole-cell currents in voltage-clamp mode. Cells were held at −70 mV. Step depolarization from −80 to +60 mV at 10-mV intervals was delivered. Inset shows Na$^+$ currents.

(I) Quantification of membrane capacitance in neurons at 60 days after differentiation. Error bars indicate ±SEM. *$p < 0.05$; a two-tailed t test was performed.

(J) Quantification of membrane resistance in neurons at 60 days after differentiation. *$p < 0.05$.

(K and L) Averaged current-voltage relationship (I-V curves) for Na$^+$ currents, recorded from hESC-derived neurons. ns, not significant; *$p < 0.05$, **$p < 0.01$.

(M and N) Averaged current-voltage relationship (I-V curves) for K$^+$ currents, recorded from hESC-derived neurons. ns, not significant; *$p < 0.05$, **$p < 0.01$.
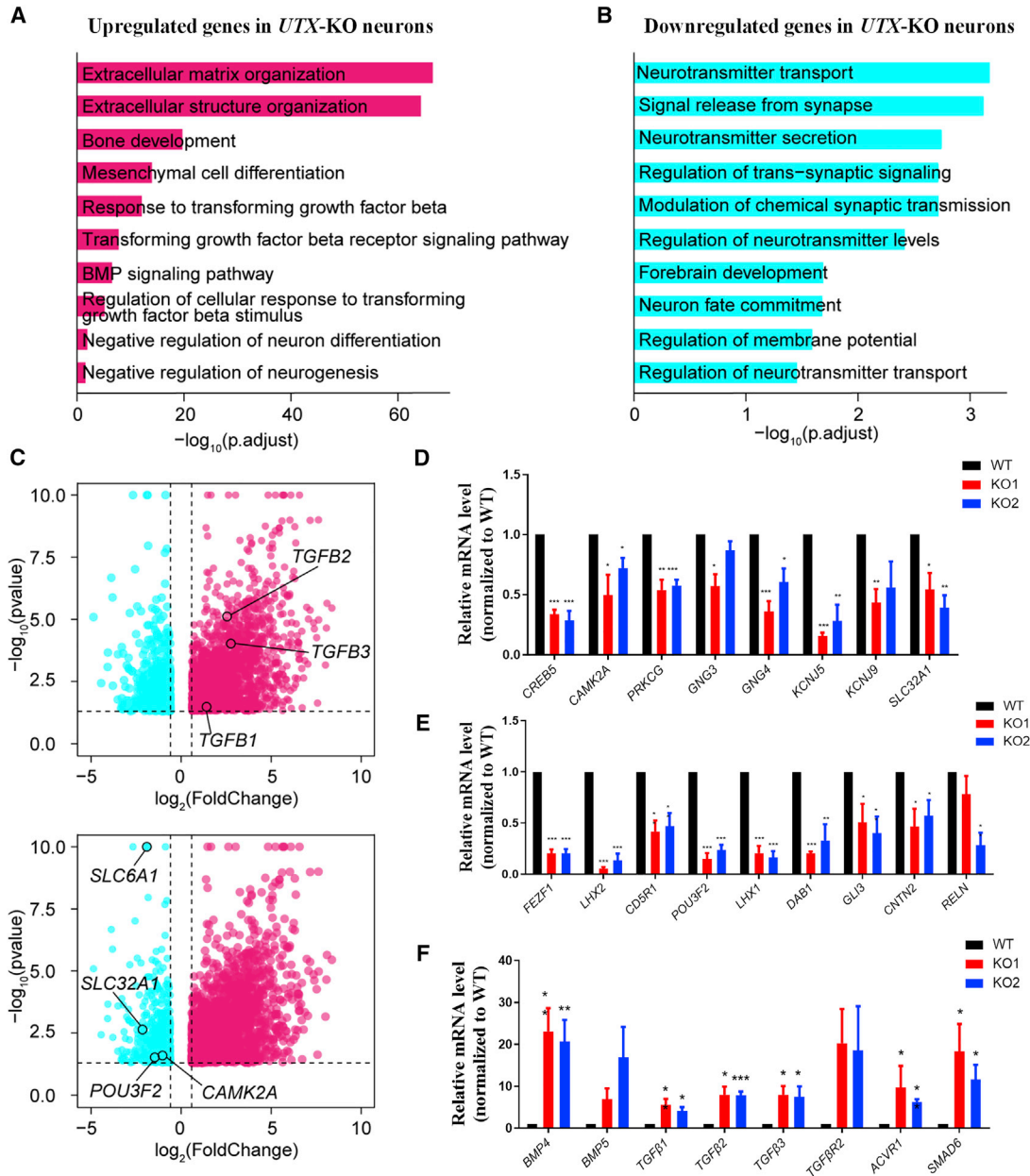
Figure 5. *UTX* KO Neurons Have an Abnormal Gene Expression Profile that Is Related to the Development and Synaptic Function

(A) Gene ontology terms enriched in genes upregulated in *UTX* KO-derived neurons.

(B) Gene ontology terms enriched in genes downregulated in *UTX* KO-derived neurons.

(C) Volcano plot of downregulated genes (blue) and upregulated genes (red) in *UTX* KO-derived neurons. Genes associated with *TGF-β* signaling pathway (*TGF-β1*, *TGF-β2*, *TGF-β3*) and neural function (*SLC6A1*, *SLC32A1*, *POU3F2*, *CAMK2A*) are indicated.

(D) qPCR analysis verified that genes positively participated in synapse-related pathways were significantly downregulated in *UTX* KO neurons.

(E) qPCR analysis verified that genes positively participated in neural development were significantly downregulated in *UTX* KO neurons.

(F) qPCR analysis verified that genes positively participated in TGF-β signaling pathway were significantly upregulated in *UTX* KO neurons.

Results are presented as mean ± SEM; n = at least 3 independent experiments. *p < 0.05, **p < 0.01, ***p < 0.001. FC, fold change.

genes in *UTX* KO neurons and NPCs. Our results showed that the H3K27me3 enrichment decreased when *UTX* WT NPCs differentiated to neurons; however, the H3K27me3 enrichment level increased in differentiated *UTX* KO neurons (Figure 7C). The H3K36me3 enrichments in gene bodies of these 70 genes were also
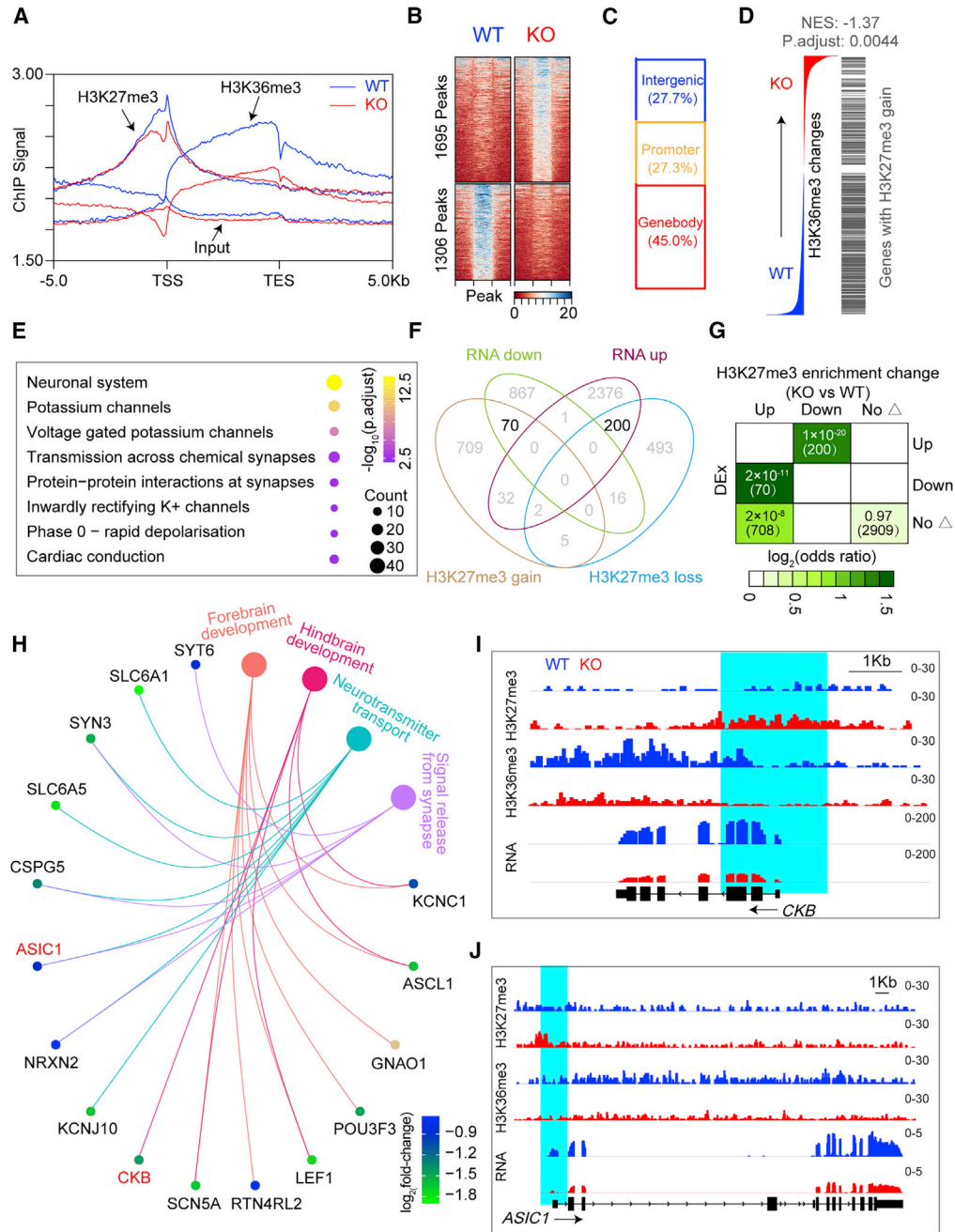
Figure 6. The Gain of H3K27me3 Associates with the Reduction of Transcription in *UTX* KO Neurons

(A) Average profiles of histone marks and input within ±5 kb of gene body of all GENCODE annotated genes.

(B) Heatmaps of H3K27me3 peaks divided into increased enrichment (1,695 peaks) and decreased enrichment (1,306 peaks) group before and after *UTX* knockout separately.

(C) Bar chart showing distribution of gained H3K27me3 peaks caused by *UTX* knockout at annotated genomic regions.

(D) Gene set enrichment analysis of association between changes of H3K27me3 and H3K36me3 changes.

(E) Reactome pathway enrichment analysis of genes with gained H3K27me3.

(F) Venn diagram of a combined comparison of differentially expressed genes (RNA-up, upregulated genes; RNA-down, downregulated genes) and genes with different H3K27me3 enrichment (H3K27me3 gain, genes with increased H3K27me3 enrichment; H3K27me3 loss, genes with decreased H3K27me3 enrichment).

decreased in *UTX* KO neurons compared with WT neurons. These results indicated that *UTX* was involved in the resolution and activation of bivalent promoters during the neural differentiation of hESCs.

DISCUSSION

Aberrant neural differentiation and dendritic morphogenesis in neurons are pervasive in many developmental brain disorders (Kulkarni and Firestein, 2012; Moretti et al., 2006). Deletion of *UTX* results in increased anxiety-like behaviors and impaired spatial learning and memory in mice, and *UTX* deficiency in the hippocampus leads to reduced long-term potentiation and amplitude of miniature excitatory postsynaptic current, aberrant dendrite development, and defective synapse formation (Tang et al., 2017). In this paper, we show that *UTX* regulates neural differentiation and dendritic morphology during the differentiation of hESCs into neurons by resolving bivalent promoters, partially through association with transcription factors. Deletion of *UTX* makes some bivalent promoters of critical genes associating with neural development to increase H3K27me3 and to reduce H3K36me3 to inhibit their transcription, which eventually causes defects in human neural differentiation, dendritic morphogenesis, and electrophysiological function (Figure 7D).

In the process of neurogenesis, we find that H3K27me3 levels were unchanged in the hESCs after the loss of *UTX*, and the differentiation potential of *UTX* KO hESCs to hNPCs is not affected. This finding supports the idea that maintaining the level of H3K27me3 may be important for the early stage of neurogenesis (Shan et al., 2020).

There is a great debate on how *UTX* regulates gene transcription. Given the role of *UTX* in removal of repressive H3K27me3 to establish transcriptionally permissive chromatin, its demethylase activity is required for activating gene expression in T cells (Manna et al., 2015), osteoblasts (Yang et al., 2015), and myoblasts (Faralli et al., 2016). A previously published study reports that human *53BP1* contains a *UTX*-binding site and the *53BP1-UTX* interaction is required to upregulate key neurodevelopmental genes during the differentiation of hESCs into neurons (Yang et al., 2019). In the present study, we provide more evidence to demonstrate that *UTX* not only regulates the transition of hNPCs to neurons, but also affects neural morphogenesis and synaptic function by resolving bivalent promoters.

UTX has been reported necessary for the resolution and activation of numerous retinoic acid (RA)-inducible bivalent genes during the RA-driven differentiation of mouse embryonic stem cells (Dhar et al., 2016). Consistent with this, we also demonstrate that *UTX* plays an important role in human neural differentiation and neural morphology by regulating bivalent promoters.

Importantly, we find that *UTX* deficiency in hESC-derived neurons also causes transcriptional activation of dozens of genes, i.e., *TGF-β* signaling pathway-related genes, including *BMP4*, *TGF-β1*, *TGF-β2*, *TGF-β3*, and *ACVR1*, which negatively regulate neuronal morphogenesis (Nakashima et al., 2018), and the inhibition of the TGF-β signaling pathway is important for the differentiation of hESCs to neurons (Morizane et al., 2011). How these genes are activated after the loss of *UTX* still needs to be studied. Interestingly, *EZH2* is downregulated in *UTX*-null hESC-derived neurons, we speculate that *EZH2* reduction may be responsible for the de-repression of upregulated genes during neural differentiation of *UTX*-null hESCs. For a better understanding of the complex regulatory mechanisms mediated by *UTX*, future studies are necessary to characterize chromatin structure and epigenetic modification by a higher resolution of both RNA and DNA sequencing.

EXPERIMENTAL PROCEDURES

Maintenance and Differentiation of hESCs

The human H9 (WA09) ESC line was obtained from Dr. Baoyang Hu at the Institute of Zoology, Chinese Academy of Sciences. H9 cells were cultured on Matrigel (BD, New Jersey, USA) using TeSR-E8 (STEMCELL Technologies, Vancouver, BC, Canada) and passaged with EDTA (100 μM). Neural differentiation of the H9 cells was initiated by the formation of embryoid bodies (EBs) as described previously with minor modifications (Jiang et al., 2013). In brief, hESC colonies were dissociated with Accutase (BD) and resuspended as single cells in E8 medium with 10 μM Rock inhibitor (Y27632, Selleck, Shanghai, China). To produce EBs from hESCs, hESC medium was replaced with N2 medium (DMEMF/12, 1× N2, 1× NEAA) at day 3 and the medium was changed every other day. To obtain NPCs derived from hESCs, the EBs were plated at day 7 on Matrigel-coated plates with 1 μg/mL laminin (Life Technologies, Carlsbad, CA, USA) and cultured in N2 medium. NPCs in the form of rosettes were manually picked at day 14 and expanded as neurospheres in N2B27 medium (DMEM/F12, 1× N2, 1× B27, 0.2 μM RA, and 20 ng/mL fibroblast growth factor 2) until day 20. For neuronal differentiation, the dissociated NPCs at day 20 were plated onto poly-L-

(G) Odds ratio analysis of overlapping genes displaying differential histone H3K27me3 enrichment versus differential gene expression (DEx), insert numbers indicate respective p values for associations, with the number of genes overlapping in parentheses.

(H) Gene ontology enrichment analysis of these 70 genes with increased H3K27me3 enrichment and downregulated expression. Displayed terms are all with an "p.adjust" < 0.05.

(I and J) Genome-browser view at *CKB* gene (I) and *ASIC1* (J) of different sequencing datasets.
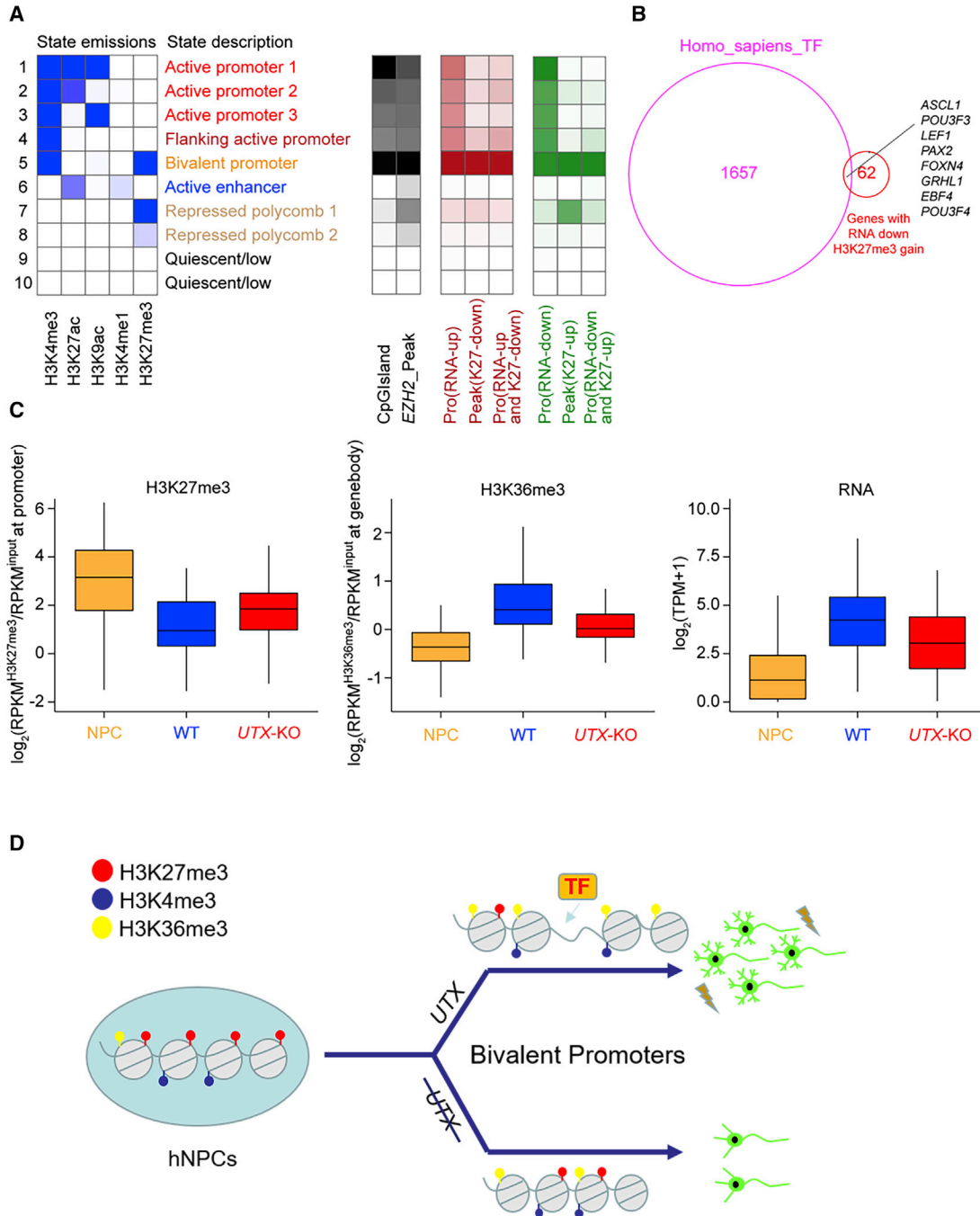
Figure 7. *UTX* Resolves Bivalent Promoters for the Induction of Lineage-Specific Genes during Human Neural Differentiation

(A) Heatmap showing distribution of indicated groups of genomic regions on the chromatin states in NPCs modeled using ChromHMM (pro, promoters).

(B) Venn diagram of a combined comparison of 70 genes with downregulated expression and H3K27me3 gain with TFs.

(C) Left panel, boxplots showing changes of promoter H3K27me3 level of different conditions of 70 genes with downregulated expression and H3K27me3 gain; middle panel, boxplots showing changes of gene body H3K36me3 level of these genes; right panel, boxplots showing gene expression changes of these genes. (ChIP-seq and RNA-seq data of neural progenitor cell originated from H9 were downloaded from ENCODE [https://www.encodeproject.org/, biosample: ENCBS044KWE] and re-analyzed.)

(D) A hypothetical model of *UTX* as a bivalency-resolving demethylase necessary for neural differentiation of hESCs.

ornithine/laminin (50 μg/mL)-coated coverslips, and cultured in neuronal differentiation medium (DMEM/F12, 1× N2, 1× B27, 10 ng/mL brain-derived neurotrophic factor, 10 ng/mL GDNF, 1 mM dibutyryl-cyclic AMP, and 200 nM ascorbic acid).

Construction of the RNA-Guided CRISPR/Cas9 Vector

Two specific guide RNA sequences (sgRNAs) targeting exon 1 of *UTX* were designed at the Optimized CRISPR Design website (http://crispr.mit.edu) (Cong et al., 2013). Then, the two guide RNA sequences were respectively annealed and cloned to the PX330-GFP-U6 plasmid (a gift from Dr. Haoyi Wang at the Institute of Zoology, Chinese Academy of Sciences) to generate all-in-one expression vector containing two sgRNA expression cassettes.

CRISPR/Cas9-Mediated KO of UTX in hESCs

H9 cells were dissociated into single cells using Accutase at 37°C for 5 min. Cells (2×10^6) were electroporated with 10 μg *UTX* double-guide RNA expression plasmid using Human Stem Cell Nucleofector kit 2 (Lonza) with program CM115 in a Nucleofector II device. Cells were resuspended in hESC medium supplemented with 10 μM Rock inhibitor (Y-27632) and re-plated on Matrigel-coated plates. After 36 h of culture, GFP-positive cells were selected with flow cytometry and reseeded as single cells. Approximately 2 weeks later, colonies were singly picked and expanded for genotype sequencing.

Histone Extraction

Histones were isolated from cells by following a standard acid extraction protocol (Shechter et al., 2007). In brief, the cells were suspended with hypotonic lysis buffer and blown into single cells. Then the cells were shaken at 4°C for 30 min and centrifuged at $10,000 \times g$ for 10 min at 4°C. Supernatant was discarded and the nuclei pellet was resuspended in 0.4 N H_2SO_4. Then the nucleic solution was centrifuged and supernatant was collected, and 132 μL tricarboxylic acid (TCA) was added drop by drop to histone solution and the tube was inverted several times to mix the solutions (the final concentration of TCA was 33%). The precipitate was centrifuged, collected and washed with acetone twice. Finally, histone was dissolved with 4 M urea.

Proliferation Analysis of Cultured NPCs

To examine the proliferation ability of NPCs, EBs at day 7 of culture were plated on Matrigel-coated coverslips. After 7 days of differentiation, 5 μM BrdU (Sigma-Aldrich, St. Louis, MO, USA) was added to the culture medium for 3.5 h. NPCs were then fixed with 4% paraformaldehyde for 20 min at room temperature, and finally washed with 1× PBS, followed by BrdU immunostaining.

In Vitro Analysis of Dendritic Morphology

For quantitative analysis of dendrites, neurons at day 40 in culture were fixed with 4% paraformaldehyde and then washed with PBS *in vitro*. Fixed neurons were blocked and permeabilized with 2% normal goat serum/0.1% Triton X-100 for 1 h at room temperature. Neurons were incubated with anti-Map2 antibody (cat. no. 822501, BioLegend, 1:1,000) overnight at 4°C, and then incubated with secondary antibody for 1 h at room temperature. Images of the dendrites were acquired using a Zeiss LSM710 confocal microscope with a 40× lens. Dendritic branches were traced, and their lengths were calculated using the Simple Neurite Tracer plugin of Fiji.

Western Blot Analysis

Cell pellets were lysed in RIPA lysis buffer (Thermo Fisher Scientific, Waltham, MA, USA) supplemented with protease inhibitor (Roche Applied Science), and samples were then quantified using a BCA protein assay kit (Thermo Fisher Scientific). After electrophoresis, proteins were transferred onto nitrocellulose membranes. The following primary antibodies were used: UTX (cat no. GTX121246, GeneTex, 1:2,000), JMJD3 (cat no. GTX124222, GeneTex 1:1,000), Oct-3/4 (cat no. sc-5279 Santa Cruz 1:1,000), and NANOG (cat no. 14295-1 Proteintech 1:1,000).

Electrophysiological Recordings

Whole-cell current and clamp recordings were performed at 22°C in artificial cerebral spinal fluid, bubbled with 95% O_2 and 5% CO_2. The extracellular fluid consisted of: 124 mM NaCl, 3.3 mM KCl, 2.4 mM $MgSO_4$, 1.2 mM KH_2PO_4, 26 mM $NaHCO_3$, 2.5 mM $CaCl_2$, and 10 mM glucose (pH 7.4). Borosilicate glass electrodes (resistance 6–10 MΩ) were filled with an intracellular solution containing 135 mM potassium gluconate, 7 mM NaCl, 10 mM HEPES, 2 mM MgATP, 0.3 mM Na_2GTP, and 2 mM $MgCl_2$, adjusted to pH 7.4 with KOH. Cell visualization and patch pipette micromanipulation were performed by video-microscopy, using a 40× water-immersion objective mounted on an upright microscope equipped with infrared differential interference contrast (Nikon, Eclipse fn1, Japan). Intracellular membrane electrical potentials were recorded in current-clamp mode, using a Multi-clamp 700B amplifier (Molecular Devices, Palo Alto, CA, USA). For voltage-clamp recordings, cells were held at −70 mV. All compounds were obtained from Sigma (St. Louis, MO). Data were digitized at 10 kHz with a 2-kHz low-pass filter. Data processing and analysis were performed using Clampfit 10.6 (Axon Instruments).

RNA Isolation and qRT-PCR

Total RNA was extracted with TRIzol (Invitrogen, New York, UK) and then was reverse-transcribed into cDNA using the TransScript One-Step gDNA Removal and cDNA Synthesis SuperMix Kit (cat no. 20200725 TRAN). Real-time qPCR was performed using the Super Real PreMix Plus (SYBR Green I) (Takara) in a 20-μL reaction system on the Roche LightCycler@480II. ACTB was used as endogenous control to normalize the RNA content of samples. The primers we used were listed in Table S1. The relative expression level of each mRNA was analyzed by the ΔΔCT method. All experiments were repeated at least in triplicate.

Statistical Analysis

Experiments were conducted in at least three biological replicates for each group. For statistical analyses, unpaired two-tailed Student's t tests (two groups) or ANOVA (three or more groups) were performed using GraphPad Prism 6.0 software. All data were presented as mean ± SEM. Differences of $p < 0.05$ were considered statistically significant.

Data and Code Availability

SUPPLEMENTAL INFORMATION

AUTHOR CONTRIBUTIONS

C.-M.L., Q.-Y.T., and Z.-Q.T., conceived and designed the study, collected, assembled, analyzed, and interpreted the data, wrote the manuscript, and approved the final manuscript. S.-F.Z., S.-K.D., C.L., Y.-Y.W., and H.-Z.D. collected and assembled the data.

ACKNOWLEDGMENTS

REFERENCES

Agger, K., Cloos, P.A., Christensen, J., Pasini, D., Rose, S., Rappsilber, J., Issaeva, I., Canaani, E., Salcini, A.E., and Helin, K. (2007). UTX and JMJD3 are histone H3K27 demethylases involved in HOX gene regulation and development. Nature *449*, 731–734.

Aldiri, I., Xu, B.S., Wang, L., Chen, X., Hiler, D., Griffiths, L., Valentine, M., Shirinifard, A., Thiagarajan, S., Sablauer, A., et al. (2017). The dynamic epigenetic landscape of the retina during development, reprogramming, and tumorigenesis. Neuron *94*, 550.

Ayata, P., Badimon, A., Strasburger, H.J., Duff, M.K., Montgomery, S.E., Loh, Y.H.E., Ebert, A., Pimenova, A.A., Ramirez, B.R., Chan, A.T., et al. (2018). Epigenetic regulation of brain region-specific microglia clearance activity. Nat. Neurosci. *21*, 1049.

Beguelin, W., Teater, M., Gearhart, M.D., Calvo Fernandez, M.T., Goldstein, R.L., Cardenas, M.G., Hatzi, K., Rosen, M., Shen, H., Corcoran, C.M., et al. (2016). EZH2 and BCL6 cooperate to assemble CBX8-BCOR complex to repress bivalent promoters, mediate germinal center formation and lymphomagenesis. Cancer Cell *30*, 197–213.

Bird, A. (2002). DNA methylation patterns and epigenetic memory. Genes Dev. *16*, 6–21.

Blanco, E., Gonzalez-Ramirez, M., Alcaine-Colet, A., Aranda, S., and Di Croce, L. (2020). The bivalent genome: characterization, structure, and regulation. Trends Genet. *36*, 118–131.

Cong, L., Ran, F.A., Cox, D., Lin, S., Barretto, R., Habib, N., Hsu, P.D., Wu, X., Jiang, W., Marraffini, L.A., et al. (2013). Multiplex genome engineering using CRISPR/Cas systems. Science *339*, 819–823.

Denissov, S., Hofemeister, H., Marks, H., Kranz, A., Ciotta, G., Singh, S., Anastassiadis, K., Stunnenberg, H.G., and Stewart, A.F. (2014). Mll2 is required for H3K4 trimethylation on bivalent promoters in embryonic stem cells, whereas Mll1 is redundant. Development *141*, 526–537.

Dhar, S.S., Lee, S.H., Chen, K., Zhu, G., Oh, W., Allton, K., Gafni, O., Kim, Y.Z., Tomoiga, A.S., Barton, M.C., et al. (2016). An essential role for UTX in resolution and activation of bivalent promoters. Nucleic Acids Res. *44*, 3659–3674.

Ezhkova, E., Lien, W.H., Stokes, N., Pasolli, H.A., Silva, J.M., and Fuchs, E. (2011). EZH1 and EZH2 cogovern histone H3K27 trimethylation and are essential for hair follicle homeostasis and wound repair. Genes Dev. *25*, 485–498.

Faralli, H., Wang, C.C., Nakka, K., Benyoucef, A., Sebastian, S., Zhuang, L.N., Chu, A., Palii, C.G., Liu, C.Y., Camellato, B., et al. (2016). UTX demethylase activity is required for satellite cell-mediated muscle regeneration. J. Clin. Invest. *126*, 1555–1565.

Grasso, C.S., Wu, Y.M., Robinson, D.R., Cao, X., Dhanasekaran, S.M., Khan, A.P., Quist, M.J., Jing, X., Lonigro, R.J., Brenner, J.C., et al. (2012). The mutational landscape of lethal castration-resistant prostate cancer. Nature *487*, 239–243.

Henriquez, B., Bustos, F.J., Aguilar, R., Becerra, A., Simon, F., Montecino, M., and van Zundert, B. (2013). Ezh1 and Ezh2 differentially regulate PSD-95 gene transcription in developing hippocampal neurons. Mol. Cell Neurosci. *57*, 130–143.

Hirabayashi, Y., Suzki, N., Tsuboi, M., Endo, T.A., Toyoda, T., Shinga, J., Koseki, H., Vidal, M., and Gotoh, Y. (2009). Polycomb limits the neurogenic competence of neural precursor cells to promote astrogenic fate transition. Neuron *63*, 600–613.

Hu, D., Garruss, A.S., Gao, X., Morgan, M.A., Cook, M., Smith, E.R., and Shilatifard, A. (2013). The Mll2 branch of the COMPASS family regulates bivalent promoters in mouse embryonic stem cells. Nat. Struct. Mol. Biol. *20*, 1093–1097.

Inoue, K., Ueno, S., and Fukuda, A. (2004). Interaction of neuron-specific K^+-Cl^- cotransporter, KCC2, with brain-type creatine kinase. FEBS Lett. *564*, 131–135.

Jadhav, U., Nalapareddy, K., Saxena, M., O'Neill, N.K., Pinello, L., Yuan, G.C., Orkin, S.H., and Shivdasani, R.A. (2016). Acquired tissue-specific promoter bivalency is a basis for PRC2 necessity in adult cells. Cell *165*, 1389–1400.

Jenuwein, T., and Allis, C.D. (2001). Translating the histone code. Science *293*, 1074–1080.

Jiang, P., Chen, C., Wang, R., Chechneva, O.V., Chung, S.H., Rao, M.S., Pleasure, D.E., Liu, Y., Zhang, Q., and Deng, W. (2013). hESC-derived Olig2+ progenitors generate a subtype of astroglia with protective effects against ischaemic brain injury. Nat. Commun. *4*, 2196.

Kruidenier, L., Chung, C.W., Cheng, Z., Liddle, J., Che, K., Joberty, G., Bantscheff, M., Bountra, C., Bridges, A., Diallo, H., et al. (2012). A selective jumonji H3K27 demethylase inhibitor modulates the proinflammatory macrophage response. Nature *488*, 404–408.

Kulkarni, V.A., and Firestein, B.L. (2012). The dendritic tree and brain disorders. Mol. Cell Neurosci. *50*, 10–20.

Lan, F., Bayliss, P.E., Rinn, J.L., Whetstine, J.R., Wang, J.K., Chen, S., Iwase, S., Alpatov, R., Issaeva, I., Canaani, E., et al. (2007). A histone H3 lysine 27 demethylase regulates animal posterior development. Nature *449*, 689–694.

Lei, X., and Jiao, J. (2018). UTX affects neural stem cell proliferation and differentiation through PTEN signaling. Stem Cell Reports *10*, 1193–1207.

Liu, J.C., Wu, X.W., Zhang, H.Y., Pfeifer, G.P., and Lu, Q. (2017). Dynamics of RNA polymerase II pausing and bivalent histone H3 methylation during neuronal differentiation in brain development. Cell Rep. *20*, 1307–1318.

Manna, S., Kim, J.K., Bauge, C., Cam, M., Zhao, Y.M., Shetty, J., Vacchio, M.S., Castro, E., Tran, B., Tessarollo, L., et al. (2015). Histone H3 Lysine 27 demethylases Jmjd3 and Utx are required for T-cell differentiation. Nat. Commun. *6*, 8152.

Mansour, A.A., Gafni, O., Weinberger, L., Zviran, A., Ayyash, M., Rais, Y., Krupalnik, V., Zerbib, M., Amann-Zalcenstein, D., Maza, I., et al. (2012). The H3K27 demethylase Utx regulates somatic and germ cell epigenetic reprogramming. Nature *488*, 409–413.

Mantsoki, A., Devailly, G., and Joshi, A. (2015). CpG island erosion, polycomb occupancy and sequence motif enrichment at bivalent promoters in mammalian embryonic stem cells. Sci. Rep. *5*, 16791.

Margueron, R., and Reinberg, D. (2011). The Polycomb complex PRC2 and its mark in life. Nature *469*, 343–349.

Minoux, M., Holwerda, S., Vitobello, A., Kitazawa, T., Kohler, H., Stadler, M.B., and Rijli, F.M. (2017). Gene bivalency at Polycomb domains regulates cranial neural crest positional identity. Science *355*, eaal2913.

Miyake, N., Mizuno, S., Okamoto, N., Ohashi, H., Shiina, M., Ogata, K., Tsurusaki, Y., Nakashima, M., Saitsu, H., Niikawa, N., et al. (2013). KDM6A point mutations cause Kabuki syndrome. Hum. Mutat. *34*, 108–110.

Moretti, P., Levenson, J.M., Battaglia, F., Atkinson, R., Teague, R., Antalffy, B., Armstrong, D., Arancio, O., Sweatt, J.D., and Zoghbi, H.Y. (2006). Learning and memory and synaptic plasticity are impaired in a mouse model of Rett syndrome. J. Neurosci. *26*, 319–327.

Morizane, A., Doi, D., Kikuchi, T., Nishimura, K., and Takahashi, J. (2011). Small-molecule inhibitors of bone morphogenic protein and activin/nodal signals promote highly efficient neural induction from human pluripotent stem cells. J. Neurosci. Res. *89*, 117–126.

Nakashima, H., Tsujimura, K., Irie, K., Ishizu, M., Pan, M., Kameda, T., and Nakashima, K. (2018). Canonical TGF-beta signaling negatively regulates neuronal morphogenesis through TGIF/Smad complex-mediated CRMP2 suppression. J. Neurosci. *38*, 4791–4810.

Pereira, J.D., Sansom, S.N., Smith, J., Dobenecker, M.W., Tarakhovsky, A., and Livesey, F.J. (2010). Ezh2, the histone methyltransferase of PRC2, regulates the balance between self-renewal and differ-

entiation in the cerebral cortex. Proc. Natl. Acad. Sci. U S A *107*, 15957–15962.

Shan, Y., Zhang, Y., Zhao, Y., Wang, T., Zhang, J., Yao, J., Ma, N., Liang, Z., Huang, W., Huang, K., et al. (2020). JMJD3 and UTX determine fidelity and lineage specification of human neural progenitor cells. Nat. Commun. *11*, 382.

Shechter, D., Dormann, H.L., Allis, C.D., and Hake, S.B. (2007). Extraction, purification and analysis of histones. Nat. Protoc. *2*, 1445–1457.

Shpargel, K.B., Starmer, J., Wang, C., Ge, K., and Magnuson, T. (2017). UTX-guided neural crest function underlies craniofacial features of Kabuki syndrome. Proc. Natl. Acad. Sci. U S A *114*, E9046–E9055.

Stewart-Morgan, K.R., Petryk, N., and Groth, A. (2020). Chromatin replication and epigenetic cell memory. Nat. Cell Biol. *22*, 361–371.

Swigut, T., and Wysocka, J. (2007). H3K27 demethylases, at long last. Cell *131*, 29–32.

Tang, G.B., Zeng, Y.Q., Liu, P.P., Mi, T.W., Zhang, S.F., Dai, S.K., Tang, Q.Y., Yang, L., Xu, Y.J., Yan, H.L., et al. (2017). The histone H3K27 demethylase UTX regulates synaptic plasticity and cognitive behaviors in mice. Front Mol. Neurosci. *10*, 267.

Tsankova, N., Renthal, W., Kumar, A., and Nestler, E.J. (2007). Epigenetic regulation in psychiatric disorders. Nat. Rev. Neurosci. *8*, 355–367.

Voigt, P., Tee, W.W., and Reinberg, D. (2013). A double take on bivalent promoters. Genes Dev. *27*, 1318–1338.

Wei, G., Wei, L., Zhu, J., Zang, C., Hu-Li, J., Yao, Z., Cui, K., Kanno, Y., Roh, T.Y., Watford, W.T., et al. (2009). Global mapping of H3K4me3 and H3K27me3 reveals specificity and plasticity in lineage fate determination of differentiating CD4+ T cells. Immunity *30*, 155–167.

Wemmie, J.A., Askwith, C.C., Lamani, E., Cassell, M.D., Freeman, J.H., and Welsh, M.J. (2003). Acid-sensing ion channel 1 is localized in brain regions with high synaptic density and contributes to fear conditioning. J. Neurosci. *23*, 5496–5502.

Xu, J., Deng, X., Watkins, R., and Disteche, C.M. (2008). Sex-specific differences in expression of histone demethylases Utx and Uty in mouse brain and neurons. J. Neurosci. *28*, 4521–4527.

Yang, D., Okamura, H., Teramachi, J., and Haneji, T. (2015). Histone demethylase Utx regulates differentiation and mineralization in osteoblasts. J. Cell Biochem. *116*, 2628–2636.

Yang, X., Xu, B., Mulvey, B., Evans, M., Jordan, S., Wang, Y.D., Pagala, V., Peng, J., Fan, Y., Patel, A., et al. (2019). Differentiation of human pluripotent stem cells into neurons or cortical organoids requires transcriptional co-regulation by UTX and 53BP1. Nat. Neurosci. *22*, 362–373.

Zhang, F., Xu, L., Xu, L., Xu, Q., Li, D., Yang, Y., Karsenty, G., and Chen, C.D. (2015). JMJD3 promotes chondrocyte proliferation and hypertrophy during endochondral bone formation in mice. J. Mol. Cell Biol. *7*, 23–34.